symmetry

IMPACT FACTOR 2.2

CITESCORE 5.4

Article

Constraint of $d = 8$ Lorentz Invariance Violation with New Experimental Design

Tao Jin, Jia-Rui Li, Yu-Jie Tan, Pan-Pan Wang, Cheng-Gang Qin and Cheng-Gang Shao

Special Issue

Lorentz Symmetry and General Relativity

Edited by

Prof. Dr. Chenggang Shao

MDPI

https://doi.org/10.3390/sym16111432

symmetry

MDPI

Article

Constraint of $d = 8$ Lorentz Invariance Violation with New Experimental Design

Tao Jin, Jia-Rui Li, Yu-Jie Tan *, Pan-Pan Wang, Cheng-Gang Qin and Cheng-Gang Shao *

MOE Key Laboratory of Fundamental Physical Quantities Measurements, Hubei Key Laboratory of Gravitation and Quantum Physics, National Precise Gravity Measurement Facility (PGMF), School of Physics, Huazhong University of Science and Technology, Wuhan 430074, China; d202080034@hust.edu.cn (T.J.); jrli@hust.edu.cn (J.-R.L.); ppwang@hust.edu.cn (P.-P.W.); cgqin@hust.edu.cn (C.-G.Q.)
* Correspondence: yjtan@hust.edu.cn (Y.-J.T.); cgshao@hust.edu.cn (C.-G.S.)

Abstract: Short-range gravity experiments are more suitable for the testing of high-order Lorentz symmetry breaking effects. In our previous work, we proposed a new experimental design based on precision torsion balance technology to test the Lorentz violation force effect that varies inversely with the fourth power of distance (corresponding to mass dimension $d = 6$ term), and the corresponding experiment is currently underway. In this paper, we focus on analyzing the potential of this experimental scheme to test the Lorentz violation force that varies inversely with the sixth power of distance (corresponding to mass dimension $d = 8$ term). The results show that, compared with the current best limit, the new experimental scheme can improve the constraints on the Lorentz violation coefficients with $d = 8$ by at least one order of magnitude.

Keywords: local Lorentz invariance violation; pure gravity sector; striped experimental design

Citation: Jin, T.; Li, J.-R.; Tan, Y.-J.; Wang, P.-P.; Qin, C.-G.; Shao, C.-G. Constraint of $d = 8$ Lorentz Invariance Violation with New Experimental Design. *Symmetry* **2024**, *16*, 1432. https://doi.org/10.3390/sym16111432

Academic Editor: Alberto Ruiz Jimeno

Received: 27 September 2024
Revised: 24 October 2024
Accepted: 25 October 2024
Published: 28 October 2024

1. Introduction

Local Lorentz invariance (LLI), an integral component of general relativity (GR), asserts that the physical outcomes remain unaltered under rotations and boosts applied to a physical system. This fundamental principle underpins the universality of physical laws within all local inertial frames of reference in the framework of GR. However, the current inability of gravity to be successfully quantized leads to a difficulty in realizing the grand unified theory, as well as the inability of dark matter and dark energy to be rationally explained, which are challenging the two fundamental theories of GR and the standard model [1–9]. Consequently, some new theories argue that this fundamental spacetime symmetry does not necessarily hold strictly and predict that the Lorentz symmetry will be broken at some extreme scales, including string theories [10], quantum gravity [11], non-commutative geometry [12] and so on [13,14]. This paper is adopts the Standard Model Expansion (SME) framework, which is an extensive and comprehensive framework for the study of the Lorentz and charge–parity–time (CPT) symmetry violation [15]. In this framework, the Lorentz violation effect is categorized into three distinct components: the purely matter sector, the purely gravitational sector, and the matter–gravitational coupled sector. These violation effects have motivated extensive research and interest, with various experiments and observations [16–25]. Among these, the purely gravitational Lorentz breaking effect is a modification of the very strong equivalence principle (SEP), a fundamental assumption of GR [26]. Thus, testing the Lorentz invariance of pure gravity represents a test of GR and an attempt in the search for a new theory of gravity.

In the SME framework, the pure gravity sector can be formulated through a Lagrange density encompassing the standard Einstein–Hilbert term R alongside a cosmological constant Λ. Additionally, it incorporates the LLI violating terms, represented by an infi-

nite series of operators characterized by an escalating mass dimension d, embodying the manifestation of LLI violation [27,28]:

$$L = \frac{\sqrt{-g}}{16\pi G_N}\left[(R - 2\Lambda) + L_M + L_{LV}^{(4)} + L_{LV}^{(5)} + L_{LV}^{(6)} + L_{LV}^{(7)} + L_{LV}^{(8)} \cdots\right]. \quad (1)$$

Here, L_M is the matter term and the latter term is the Lorentz violation term. Since there are no non-relativistic gravitational effects when d is odd, only the case in which the mass dimension d is even is considered here. The minimum coupling term corresponds to violating potential with $d = 4$ that is inversely proportional to the distance r between the test mass and source mass, while the violating potential of the higher-order coupling terms $d \geq 6$ is inversely proportional to the higher-order terms such as 3, 5, and 7 of the distance. Therefore, short-range gravity experiments are sensitive to the testing of higher-order Lorentz violation effects. At present, the best limits on high-order coupling terms come from Huazhong University of Science and Technology (HUST) and Indiana University (IU). They collaboratively analyzed data from short-range inverse square law test experiments, including HUST-2012 [29] and HUST-2015 [30] conducted by HUST and IU-2002 and IU-2012 from IU [31]. These analyses provided the most stringent constraints on the violation coefficients for the higher-order term with d = 6 at the level of 10^{-9} m^2 [32] and for the higher-order term with d = 8 at the level of 10^{-12} m^4 [33]. Considering that the above experiments were mainly designed to test the Yukawa model, the experimental setup is relatively sensitive for the exploration of the parameters related to this model, but it may not necessarily be sufficiently sensitive to research the Lorentz violating effects. Therefore, the research team further investigated experimental schemes specifically targeted at testing Lorentz violation, and they found that that the $d = 6$ Lorentz violating term was sensitive to the edge effect. They further proposed a new torsion pendulum experimental scheme with a stripe-type structure test mass and source mass (as shown in Figure 1) to amplify the edge effect [34], in order to carry out a higher-level test of the d = 6 violating term. The corresponding experiment is proceeding smoothly [35].

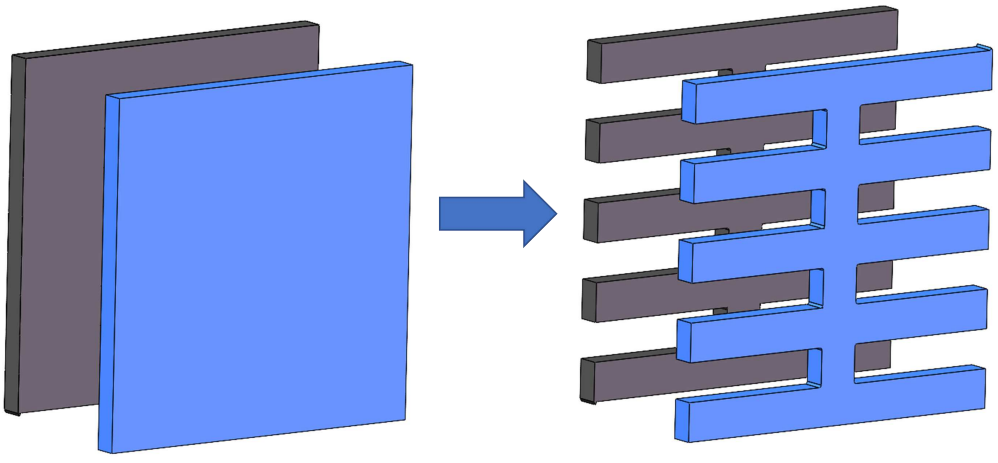

Figure 1. Test mass and source mass with stripe-type structure. The most stringent constraints all came from the short-range inverse square law test experiments, in which the test mass and source mass were of a flat plate structure (shown in (**a**)). The new experiment was designed with the test mass and source mass in a stripe-type structure to enhance the Lorentz violating signal (shown in (**b**)).

Considering that the best tests of d = 8 Lorentz violating terms come from the analysis of experimental data on Newton's inverse square law [33,36], the experimental configuration is sensitive to the Yukawa model but not necessarily sensitive to the relevant Lorentz violating effects of d = 8. However, the torsion pendulum experimental scheme proposed earlier, specifically for the test of d = 6 violating effects, may also be sensitive for the testing of d = 8 violating terms. Therefore, in order to refine the application of the proposed new

experimental scheme, this paper will analyze the potential of the stripe-type design scheme for the testing of the Lorentz violating effects for d = 8.

2. Principle Analysis of Constraint d = 8 LLI with Torsion Pendulum Experiments

For the Lorentz violating effects in the purely gravitational part, the SME framework develops a spherical coordinate representation, which can be used to describe uniformly the Lorentz violating force effects that are inversely proportional to the distance in quadratic, quartic, sextic or even higher quadratic terms. Considering the existence of Lorentz symmetry breaking in the spherical coordinate system with mass dimension d, the Lorentz violating gravitationally modified potential between two point masses m_1, m_2 in the laboratory coordinate system can be expressed as [25]

$$U_{\mathrm{LV}}(\vec{r}) = -G\sum_{djm}\frac{m_1 m_2}{|\vec{r}|^{d-3}}Y_{jm}(\theta,\phi)k_{jm}^{N(d)Lab}, \tag{2}$$

where $\vec{r} = \vec{r}_1 - \vec{r}_2 \equiv (rcos\phi sin\theta, rsin\phi sin\theta, rcos\theta)$ denotes the position vector between two point masses m_1 and m_2; $d \geq 4$ and is even; $j = d-2$ or $d-4$; and m is an integer in the range $-j \leq m \leq j$. Given the occurrence of $d-3$ negative power corrections to the distance in Equation (2), the use of short-range gravity experiments to test higher-order Lorentz violating effects is of great advantage.

For the effect of the Lorentz violation force that is inversely proportional to the sixth power of the distance, i.e., $d = 8$, the Lorentz violating gravitational correction potential between two point masses m_1, m_2 in the laboratory reference system can be written as [33]

$$U_{\mathrm{LV}}^{d=8}(\vec{r}) = -G\sum_{jm}\frac{m_1 m_2}{|\vec{r}|^5}Y_{jm}(\theta,\phi)k_{jm}^{N(8)Lab}, \tag{3}$$

where $j =$ 6 or 4, $-j \leq$ m $\leq j$; the spherical harmonic function $Y_{jm}(\theta,\phi)$ corresponds to the basis vectors in the spherical coordinate system; and $k_{jm}^{N(8)Lab}$ are the Lorentz violating coefficients in the laboratory spherical coordinate system. For the spherical harmonic function $Y_{jm}(\theta,\phi)$, it can be expanded into an easy-to-handle tensor expression using the symmetric traceless tensor [37]. The following is the expansion:

$$Y_{lm}(\theta,\phi) = c_{lm}^{*<K>}n_{<K>}(x,y,z), \tag{4}$$

where the parameter $n_{<K>}(x,y,z)$ has the specific form

$$n_{<K>}(x,y,z) = \frac{r^{k+1}}{(-1)^k(2k-1)!!}\partial_k\frac{1}{r} \tag{5}$$

with ∂_K denoting the partial derivative $\partial_{k_1}\cdots\partial_{k_j}$. Tensor $c_{lm}^{<K>}$, consisting of the summation of all k pairs of repeated indicators, is expressed as

$$c_{lm}^{<K>} = \frac{(2k+1)!!}{4\pi k!}\int n^{<K>}Y_{lm}^{*}(\theta,\phi)d\Omega. \tag{6}$$

Based on this, the 22 spherical coordinate basis vectors involved in Equation (2) can be given.

Due to the influence of the Earth's motion, the laboratory location and azimuth angle are constantly changing; therefore, the violating coefficients under different laboratory reference frames are different. In this way, the violating coefficients given by different experimental groups in their respective laboratory reference frames are not comparable. Fortunately, under the framework of SME, the Lorentz violating coefficients are constants in the Sun-centered reference frame. To facilitate comparisons of results among different research groups, the violating coefficients are typically transformed from the laboratory

coordinate system to the Sun-centered coordinate system. This transformation process involves a series of rotations. Combining the transformation relationship between the laboratory and Sun-centered coordinate systems, the conversion between the violating coefficients in the two coordinate systems can be obtained as follows [38]:

$$k_{jm}^{N(8)Lab} = \sum_{m'} e^{im'\omega_{\oplus}T_{\oplus}} d_{mm'}^{(j)}(-\chi) k_{jm'}^{N(8)}. \tag{7}$$

Here, $k_{jm}^{N(8)Lab}$ and $k_{jm'}^{N(8)Lab}$ represent the Lorentz violating spherical coefficients in the laboratory and Sun-centered coordinate systems, respectively; $\omega_{\oplus}$ is the Earth's sidereal rotation angular frequency; $T_{\oplus}$ is the local sidereal time of the laboratory; and χ is the colatitude of the laboratory location. Combining Equations (3) and (7), one can obtain the Lorentz violating gravitational potential between two masses m_1 and m_2 in the Sun-centered coordinate system, which can be expanded in the form of a Fourier series as follows:

$$U_{\mathrm{LV}}^{d=8} = -G\frac{m_1 m_2}{r^5}(c_0 + \sum_{m=1}^{6}[c_m cos(m\omega_{\oplus}T_{\oplus}) + s_m sin(m\omega_{\oplus}T_{\oplus})]). \tag{8}$$

By substituting Equations (7) and (4) into Equation (3), the 13 Fourier amplitudes involved in Equation (8) can be expressed as a linear combination of the 22 Lorentz violating coefficients in the Sun-centered coordinate system [33]:

$$\begin{aligned}
c_0 &= \alpha_1 k_{4,0}^{N(8)} + \alpha_2 k_{6,0}^{N(8)} \\
c_2 &= \alpha_3 \mathrm{Re}k_{4,2}^{N(8)} + \alpha_4 \mathrm{Im}k_{4,2}^{N(8)} + \alpha_5 \mathrm{Re}k_{6,2}^{N(8)} + \alpha_6 \mathrm{Im}k_{6,2}^{N(8)} \\
s_2 &= \alpha_4 \mathrm{Re}k_{4,2}^{N(8)} - \alpha_3 \mathrm{Im}k_{4,2}^{N(8)} + \alpha_6 \mathrm{Re}k_{6,2}^{N(8)} - \alpha_5 \mathrm{Im}k_{6,2}^{N(8)} \\
c_4 &= \alpha_7 \mathrm{Re}k_{4,4}^{N(8)} + \alpha_8 \mathrm{Im}k_{4,4}^{N(8)} + \alpha_9 \mathrm{Re}k_{6,4}^{N(8)} + \alpha_{10} \mathrm{Im}k_{6,4}^{N(8)} \\
s_4 &= \alpha_8 \mathrm{Re}k_{4,4}^{N(8)} - \alpha_7 \mathrm{Im}k_{4,4}^{N(8)} + \alpha_{10} \mathrm{Re}k_{6,4}^{N(8)} - \alpha_9 \mathrm{Im}k_{6,4}^{N(8)} \\
c_6 &= \alpha_{11} \mathrm{Re}k_{6,6}^{N(8)} + \alpha_{12} \mathrm{Im}k_{6,6}^{N(8)} \\
s_6 &= \alpha_{12} \mathrm{Re}k_{6,6}^{N(8)} - \alpha_{11} \mathrm{Im}k_{6,6}^{N(8)} \\
c_1 &= \alpha_{13} \mathrm{Re}k_{4,1}^{N(8)} + \alpha_{14} \mathrm{Im}k_{4,1}^{N(8)} + \alpha_{15} \mathrm{Re}k_{6,1}^{N(8)} + \alpha_{16} \mathrm{Im}k_{6,1}^{N(8)} \\
s_1 &= \alpha_{14} \mathrm{Re}k_{4,1}^{N(8)} - \alpha_{13} \mathrm{Im}k_{4,1}^{N(8)} + \alpha_{16} \mathrm{Re}k_{6,1}^{N(8)} - \alpha_{15} \mathrm{Im}k_{6,1}^{N(8)} \\
c_3 &= \alpha_{17} \mathrm{Re}k_{4,3}^{N(8)} + \alpha_{18} \mathrm{Im}k_{4,3}^{N(8)} + \alpha_{19} \mathrm{Re}k_{6,3}^{N(8)} + \alpha_{20} \mathrm{Im}k_{6,3}^{N(8)} \\
s_3 &= \alpha_{18} \mathrm{Re}k_{4,3}^{N(8)} - \alpha_{17} \mathrm{Im}k_{4,3}^{N(8)} + \alpha_{20} \mathrm{Re}k_{6,3}^{N(8)} - \alpha_{19} \mathrm{Im}k_{6,3}^{N(8)} \\
c_5 &= \alpha_{21} \mathrm{Re}k_{6,5}^{N(8)} + \alpha_{22} \mathrm{Im}k_{6,5}^{N(8)} \\
s_5 &= \alpha_{22} \mathrm{Re}k_{6,5}^{N(8)} - \alpha_{21} \mathrm{Im}k_{6,5}^{N(8)}.
\end{aligned} \tag{9}$$

Here, due to the complex conjugate relationship of Lorentz violating spherical coefficients,

$$k_{jm}^{N(8)*} = (-1)k_{j(-m)}^{N(8)}, \tag{10}$$

the violating coefficients can be represented using the real part $\mathrm{Re}k_{jm}^{N(8)}$ and the imaginary part $\mathrm{Im}k_{jm}^{N(8)}$ of $k_{jm}^{N(8)}$. The detailed expressions of the 22 independent functions α_j ($j = 1, \ldots, 14$) can be found in [33].

According to Equation (2), short-range gravity experiments are highly suitable for the testing of the high-order Lorentz violation effect. Therefore, torsion pendulum experiments can be used to explore the Lorentz violation force that is inversely proportional to the sixth power of the distance. In these experiments, the violating coefficients are effectively

constrained by accurately measuring the Lorentz violating torque and extracting the corresponding amplitude signals, and the limiting accuracy of the violating coefficients depends on the experimental torque resolution level. Assuming that the elemental mass of the test mass and source mass is, respectively, $dm_1 = \rho_1 dV_1$ and $dm_2 = \rho_2 dV_2$, where ρ_1 and ρ_2, dV_1 and dV_2 are the corresponding densities and volume elements of the test mass and source mass, the Lorentz violation torque can be expressed in terms of violating coefficients in the following form:

$$\tau_{LV} = G\rho_1\rho_2 \iint dV_1 dV_2 \frac{\partial}{\partial\theta_1} \frac{\sum\limits_{jm} Y_{jm}(\theta,\phi) k_{jm}^{N(8)Lab}}{r^5} \tag{11}$$

with the transfer function being

$$\Gamma_j = G\rho_1\rho_2 \iint \frac{\partial}{\partial\theta_1} \frac{\alpha_j(\theta,\hat{r},\chi)}{r^5} dV_1 dV_2. \tag{12}$$

It can be seen that the transfer function $\Gamma_j (j = 1, 2, \ldots, 22)$ is closely related to the geometric shape parameters of the test mass and source mass, the placement of the experimental setup, and the local colatitude of the laboratory. Substituting Equation (8) into Equation (11) yields

$$\tau_{LV} = G\rho_1\rho_2 \iint dV_1 dV_2 \frac{\partial}{\partial\theta_1} \frac{c_0 + \sum\limits_{m=1}^{6} c_m \cos(m\omega_\oplus T) + s_m \sin(m\omega_\oplus T)}{r^5}. \tag{13}$$

Therefore, the Lorentz violation torque can be simply represented in the form of a Fourier series as

$$\tau_{LV} = C_0 + \sum_{m=1}^{6} [C_m cos(m\omega_\oplus T) + S_m sin(m\omega_\oplus T)]. \tag{14}$$

The specific relationship between Fourier amplitudes C_0, C_m, S_m and the violating coefficients can be given similarly to formula (9), by simply replacing c_0, c_m, s_m with C_0, C_m, S_m and α_j with Γ_j.

In the SME framework, the total number of violating coefficients is $4d - 10$, while, according to Equation (8), the maximum number of Fourier amplitudes signals that can be provided by any single experiment is only $2d - 3$. Obviously, for a single experiment, the number of violating coefficients to be constrained is much larger than the number of signals. Therefore, it is more suitable to adopt a joint analysis method to study the effect of Lorentz violating forces that vary inversely with the distance to the power of $d - 2$. Specifically, for the Lorentz violating force effect that varies inversely with the distance to the sixth power, only 13 violation signal amplitudes can be obtained in a single experiment. Although these 13 different amplitudes are composed of 22 independent violating coefficients in the form of linear combinations, they are not sufficient to independently constrain all 22 violating coefficients. Therefore, at least two sets of different experimental data need to be combined for joint analysis in order to independently constrain each violating coefficient. Our research group previously proposed an experimental test scheme specifically designed for the d = 6 Lorentz violation effect. This scheme leverages the characteristic that the transfer function is correlated with the experimental azimuth angle θ. By employing a specific experimental setup, two sets of experimental data are collected at distinct azimuth angles, θ_1 and θ_2, respectively. Subsequently, these two sets of data are combined and analyzed to independently constrain the 14 Lorentz violating coefficients. Notably, this experimental test scheme is not only applicable to the study of the d = 6 Lorentz violating effect but can also be extended to analyze and impose constraints on the d = 8 Lorentz violating effect. The following section is a brief introduction to the previous experimental scheme.

3. Experimental Scheme for Testing of LLI Effects Based on Precision Torsion Pendulum Technology

For the Lorentz violation effect with $d = 6$, we found that the violation force between infinite plates is 0 [34], leading to the conclusion that the violating effect between finite-sized objects is dominated by the edge effect. Therefore, we designed striped tungsten sheets as the test and source masses and intentionally created a half-stripe misalignment between the directly facing stripes of the test and source masses, in order to amplify the edge effect. The tungsten sheets were placed centrosymmetrically at both ends of the torsion pendulum and rotationally symmetrically at both ends of the source mass, so that, when the source mass was modulated back and forth, the Newtonian gravitational torque was always 0, and the Lorentz violating effect varied with the distance.

Based on the above, in order to provide independent constraints on the violation coefficients, it is necessary to jointly analyze data from two separate experiments. Therefore, two experiments need to be constructed. Given that the violation coefficients are sensitive to the direction, two methods for the construction of the two experiments are proposed. One is to change the orientation of the stripes, as shown in Figure 2a,b, conducting one experiment with horizontally striped test and source masses and another experiment with vertically striped ones. The other is to keep the stripe orientation unchanged and vary the azimuth angle of the experimental setup, i.e., using either horizontally or vertically striped structures for both the test masses and source masses, conducting one experiment at azimuth angle θ_1 and another at azimuth angle θ_2. Specifically, one can adopt the horizontal stripe design shown in Figure 2a, changing the azimuth angle θ and constructing two experiments for analysis. Alternatively, the vertical stripe design shown in Figure 2b can be employed, with similar operations and analyses conducted accordingly. In this method, the two optimal azimuth angles should be selected for the experiments. A detailed description of the experimental scheme can be found in [39,40]. For these two strategies, by combining the current experimental technology level and related parameter design, corresponding constraints on the violation coefficients can be obtained. Based on the previous comparative analysis, and in consideration of the difficulty in conducting the experiments, the second strategy is more suitable. It is expected to improve the $d = 6$ violating coefficients by about an order of magnitude [40].

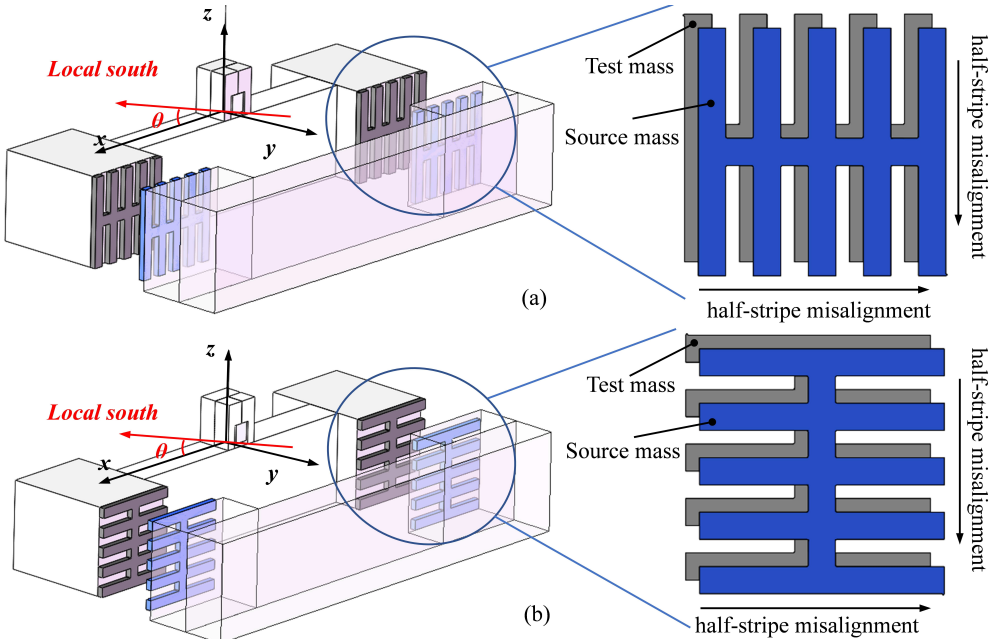

Figure 2. Experimental scheme for testing of Lorentz violation based on changing the stripe orientation and azimuth angle θ. (**a**,**b**) correspond to the cases of horizontal stripes and vertical stripes, respectively.

The overall experimental setup diagram is shown in Figure 3; it consists of the angle measuring system, the drive modulation system, the calibration system, the environmental monitoring systems, an attractor, and a pendulum. The membrane frames and the attractor are attached to a six-degrees-of-freedom stage (not depicted here). An autocollimator measures the twist of the pendulum, which is adjusted using two differential capacitive actuators. A rotating copper cylinder is utilized to calibrate the sensitivity of the pendulum. The BeCu membranes minimize the spurious torques from the electrical force between the test mass and source mass. By machining and assembling the pendulum and attractor on a micrometer scale, the entire system can exhibit sensitivity to 5×10^{-16} Nm.

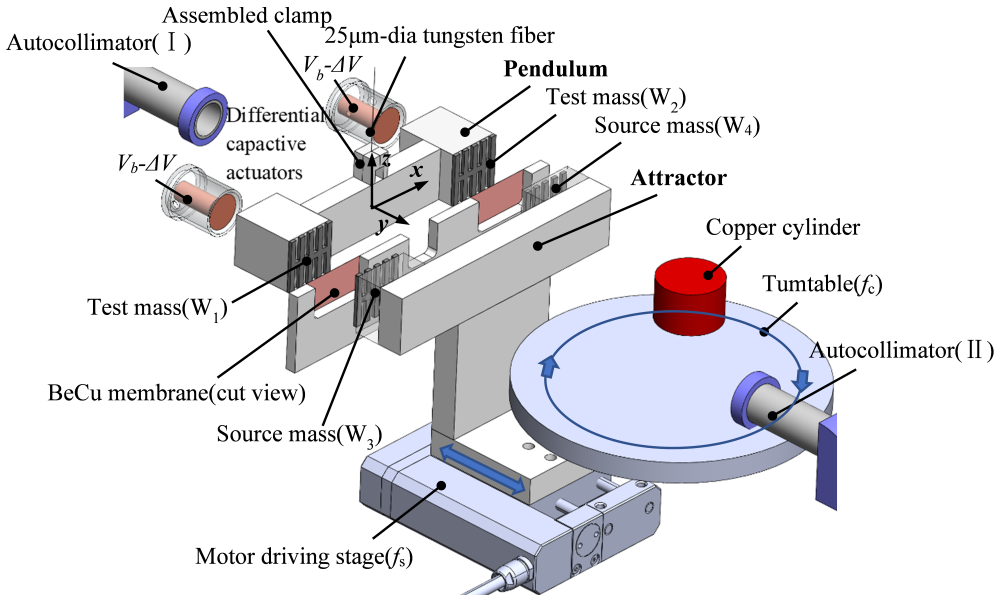

Figure 3. Schematic diagram of the Lorentz violating test experimental setup (not to scale).

Although the original intention in designing this experimental scheme was to improve the detection level of $d = 6$ Lorentz violation effects, both $d = 6$ and $d = 8$ Lorentz violation effects belong to the pure gravitational part of Lorentz violation. Therefore, this scheme may also potentially enhance the detection of $d = 8$ violation terms. In the following section, we will focus on analyzing the potential of this scheme to constrain the $d = 8$ related violation coefficients.

4. Expected Constraints on $d = 8$-Related Lorentz Violation Coefficients

Here, we analyze the scheme of constructing two experiments by changing the azimuth angle of the experimental setup while keeping the stripe orientation unchanged, in order to constrain the $d = 8$ violation coefficients. Specifically, this can be divided into two cases: using horizontal stripes and selecting two optimal azimuth angles to construct two experiments and employing vertical stripes with a similar selection of azimuth angles.

For both of the above cases, the process of obtaining constraints on the Lorentz violation coefficients is similar. First, by combining the theoretical model of the sixth-order inverse square Lorentz violation force, the design parameters of the geometric sizes of the test mass and source mass in the experimental scheme, the latitude of the laboratory, and the values of the two azimuth angles of the experimental device, the transfer function values of the various violation coefficients can be obtained. Then, taking the component processing level, environmental control level, and experimental background test level of similar experiments currently carried out in the laboratory as a reference—specifically, using the Lorentz violation amplitude signal data extracted from the HUST-2015 experiment as a reference to assess the central value of the violation coefficient, and the error analysis of the HUST-2012 experiment as a reference for error assessment—and by combining the corresponding transfer function values, the constraints of the experimental scheme on the

$d = 8$ Lorentz violation coefficient can be obtained. Below, we separately analyze and discuss the constraints on the violation coefficients under the two stripe orientation schemes.

For the horizontal stripe orientation scheme, the corresponding parameter design can be found in [40]. The two optimal experimental azimuth angles are set as $\theta = \pi/7, \pi/2$, and the values of the transfer function for each violating coefficient $\Gamma_j (j = 1, 2, \ldots, 22)$ can be obtained, as shown in Table 1. We use the two sets of Lorentz violating amplitude signal data extracted from the HUST-2015 experiment at 8- and 16-harmonic frequencies (shown in Table 2) [33] as a reference for the evaluation of the central values of the violating coefficients, and the error analysis of the HUST-2012 experiment [29,40] as a reference for the error evaluation, respectively. For the case of horizontal stripes, combining the current technology level, it is reasonable to set the error of the constant term C_0 as 11.7×10^{-16} Nm and the error of the harmonic frequency terms C_m and S_m as 0.45×10^{-16} Nm. Based on the above parameters, the constraint level of the horizontal stripe scheme for the $d = 8$ Lorentz violation coefficient can be obtained, as shown in Table 3.

For the vertical stripe orientation scheme, the corresponding parameter design can be also found in [40]. The two optimal experimental azimuth angles are set as $\theta = \pi/6, 3\pi/5$, and the values of the transfer function for each violating coefficient Γ_j $(j = 1, 2, \ldots, 22)$ can be obtained, as shown in Table 4. Similarly, we use the data in Table 2 to evaluate the central values of the violating coefficient. For the vertical stripe experimental scheme, due to the smaller alignment error in the vertical stripe design compared to the horizontal stripe design, the error of its constant term C_0 is conservatively set to be 10.4×10^{-16} Nm. For the harmonic frequency terms C_m and S_m, their expected errors are set to be 10.4×10^{-16} Nm. By substituting the aforementioned parameters, we ultimately obtain the expected constraints on the $d = 8$ Lorentz violating spherical coefficients, as presented in Table 5.

Table 1. Transfer coefficients Γ_j in horizontal stripe design ($\pm 0.01, 10^{-4}$ Nm/m^4).

Transfer Coefficient	$\theta_1 = \pi/7$	$\theta_2 = \pi/2$	Transfer Coefficient	$\theta_1 = \pi/7$	$\theta_2 = \pi/2$
Γ_1	2.06	−9.92	Γ_{12}	−5.92	−13.13
Γ_2	12.89	18.39	Γ_{13}	−11.78	9.47
Γ_3	1.45	−7.57	Γ_{14}	−0.61	3.65
Γ_4	3.38	−1.51	Γ_{15}	2.44	11.23
Γ_5	16.46	35.40	Γ_{16}	24.95	25.68
Γ_6	4.45	2.91	Γ_{17}	3.94	−5.31
Γ_7	12.35	29.30	Γ_{18}	−0.83	−1.19
Γ_8	−2.51	−3.23	Γ_{19}	−11.39	7.22
Γ_9	18.77	17.15	Γ_{20}	10.65	14.45
Γ_{10}	10.40	2.27	Γ_{21}	16.64	13.20
Γ_{11}	15.61	−15.96	Γ_{22}	1.34	−1.24

Table 2. Fourier amplitude signals extracted from HUST-2015 experiment (10^{-16} Nm).

Signal	$8f_0$	$16f_0$	Signal	$8f_0$	$16f_0$	Signal	$8f_0$	$16f_0$
C_0	0.08	−0.20	C_1	−0.03	<0.01	S_1	0.03	<0.01
			C_2	<0.01	−0.01	S_2	−0.06	−0.08
			C_3	<0.01	0.01	S_3	0.03	−0.06
			C_4	<0.01	0.04	S_4	0.01	−0.03
			C_5	0.02	−0.03	S_5	−0.08	0.05
			C_6	0.04	−0.04	S_6	<0.01	0.02

Table 3. Expected constraint level for $d = 8$ Lorentz violating coefficients under the horizontal stripe design (2σ, unit 10^{-14} m^4).

Violating Coefficient	Expected Result	Violating Coefficient	Expected Result
$k_{4,0}^{N(8)}$	2.44 ± 158.52	$k_{6,0}^{N(8)}$	0.23 ± 71.52
$\mathrm{Re}k_{4,1}^{N(8)}$	0.09 ± 2.98	$\mathrm{Im}k_{4,1}^{N(8)}$	0.19 ± 2.98
$\mathrm{Re}k_{4,2}^{N(8)}$	-0.24 ± 7.16	$\mathrm{Im}k_{4,2}^{N(8)}$	0.21 ± 7.16
$\mathrm{Re}k_{4,3}^{N(8)}$	-0.04 ± 6.60	$\mathrm{Im}k_{4,3}^{N(8)}$	-0.95 ± 6.60
$\mathrm{Re}k_{4,4}^{N(8)}$	0.16 ± 2.71	$\mathrm{Im}k_{4,4}^{N(8)}$	0.20 ± 2.71
$\mathrm{Re}k_{6,1}^{N(8)}$	-0.03 ± 1.23	$\mathrm{Im}k_{6,1}^{N(8)}$	-0.07 ± 1.23
$\mathrm{Re}k_{6,2}^{N(8)}$	-0.09 ± 1.56	$\mathrm{Im}k_{6,2}^{N(8)}$	0.27 ± 1.56
$\mathrm{Re}k_{6,3}^{N(8)}$	-0.06 ± 1.99	$\mathrm{Im}k_{6,3}^{N(8)}$	0.01 ± 1.99
$\mathrm{Re}k_{6,4}^{N(8)}$	0.03 ± 3.15	$\mathrm{Im}k_{6,4}^{N(8)}$	-0.19 ± 3.15
$\mathrm{Re}k_{6,5}^{N(8)}$	-0.05 ± 2.06	$\mathrm{Im}k_{6,5}^{N(8)}$	0.16 ± 2.06
$\mathrm{Re}k_{6,6}^{N(8)}$	0.14 ± 1.66	$\mathrm{Im}k_{6,6}^{N(8)}$	0.09 ± 1.66

Table 4. Transfer coefficients Γ_j in vertical stripe design ($\pm 0.01, 10^{-4}$ Nm/m^4).

Transfer Coefficient	$\theta_1 = \pi/6$	$\theta_2 = 3\pi/5$	Transfer Coefficient	$\theta_1 = \pi/6$	$\theta_2 = 3\pi/5$
Γ_1	2.56	−0.49	Γ_{12}	−0.86	−0.21
Γ_2	5.72	−1.74	Γ_{13}	−5.37	3.54
Γ_3	3.73	−8.07	Γ_{14}	−2.13	0.37
Γ_4	1.64	−1.77	Γ_{15}	0.03	−1.99
Γ_5	7.37	−1.72	Γ_{16}	1.50	−0.31
Γ_6	0.10	−0.03	Γ_{17}	1.69	−1.56
Γ_7	5.98	8.24	Γ_{18}	−3.80	2.08
Γ_8	−4.21	−0.82	Γ_{19}	2.77	−2.30
Γ_9	0.55	4.45	Γ_{20}	0.15	0.30
Γ_{10}	0.70	−0.19	Γ_{21}	−1.26	2.24
Γ_{11}	−1.16	−4.35	Γ_{22}	0.76	−0.85

Table 5. Expected constraint level of $d = 8$ Lorentz violating coefficients under the vertical stripe design (2σ, unit 10^{-14} m^4).

Violating Coefficient	Expected Result	Violating Coefficient	Expected Result
$k_{4,0}^{N(8)}$	6.64 ± 3764.80	$k_{6,0}^{N(8)}$	-6.47 ± 1641.28
$\mathrm{Re}k_{4,1}^{N(8)}$	0.44 ± 10.34	$\mathrm{Im}k_{4,1}^{N(8)}$	-0.40 ± 10.34
$\mathrm{Re}k_{4,2}^{N(8)}$	0.23 ± 6.16	$\mathrm{Im}k_{4,2}^{N(8)}$	-1.05 ± 6.16
$\mathrm{Re}k_{4,3}^{N(8)}$	1.23 ± 38.19	$\mathrm{Im}k_{4,3}^{N(8)}$	-0.64 ± 38.19
$\mathrm{Re}k_{4,4}^{N(8)}$	0.70 ± 6.13	$\mathrm{Im}k_{4,4}^{N(8)}$	-0.14 ± 6.13
$\mathrm{Re}k_{6,1}^{N(8)}$	2.05 ± 27.91	$\mathrm{Im}k_{6,1}^{N(8)}$	1.03 ± 27.91
$\mathrm{Re}k_{6,2}^{N(8)}$	-0.04 ± 7.50	$\mathrm{Im}k_{6,2}^{N(8)}$	1.67 ± 7.50
$\mathrm{Re}k_{6,3}^{N(8)}$	-1.31 ± 51.71	$\mathrm{Im}k_{6,3}^{N(8)}$	0.79 ± 51.71
$\mathrm{Re}k_{6,4}^{N(8)}$	-1.31 ± 14.92	$\mathrm{Im}k_{6,4}^{N(8)}$	-0.04 ± 14.92
$\mathrm{Re}k_{6,5}^{N(8)}$	2.38 ± 15.67	$\mathrm{Im}k_{6,5}^{N(8)}$	2.56 ± 15.67
$\mathrm{Re}k_{6,6}^{N(8)}$	-0.69 ± 9.59	$\mathrm{Im}k_{6,6}^{N(8)}$	0.23 ± 9.59

Tables 3 and 5 demonstrate the analysis of the $d = 6$ Lorentz violation effect test scheme proposed by our group, examining its constraints on the $d = 8$ Lorentz violation effect. Compared with the current international optimal constraint results [33], it can be seen that

the expected level of constraint on the violation coefficients can be improved by one to two orders of magnitude, which means that the scheme proposed is also suitable for the testing of the $d = 8$ Lorentz violation effect. This is mainly because the current constraint level of $d = 8$ violating coefficients is based on the experimental data of Newton's inverse square test for the testing of the Yukawa model, which, to some extent, suppresses the purely gravitational component of Lorentz symmetry violation effects. In contrast, the scheme proposed by our group focuses specifically on testing the purely gravitational component of Lorentz violation effects, making it more targeted and enhancing its sensitivity to Lorentz violation effects through experimental design.

5. Summary

Lorentz symmetry is one of the fundamental principles of modern physics, and the study of Lorentz symmetry tests is crucial for a comprehensive understanding of the basic laws of the universe. In previous research, based on the mature torsion pendulum experiment technology developed at HUST, our group has conducted a series of tests on Newton's inverse square law. Based on the relevant experimental data, we have provided the best level of constraints on Lorentz invariance violation. Furthermore, we have analyzed the characteristics of the $d = 6$ Lorentz violation effect in torsion balance experiments and proposed a targeted experimental test scheme. Through the anticipated data analysis, we believe that good constraints can be placed on the $d = 6$ Lorentz violation coefficients. In the study of the $d = 8$ Lorentz violation effect, we have discovered that this experimental scheme can also be applied to analyze the $d = 8$ Lorentz violation effect. Therefore, an exploratory analysis of the potential constraints imposed by the short-range gravitational experimental scheme designed to test the $d = 6$ Lorentz violation effect on the $d = 8$ violation effect has been conducted in this paper, to further expand the application value of the experimental scheme. The research results show that the scheme also performs well in the $d = 8$ Lorentz violation effect test, and the expected constraint level can be one to two orders of magnitude better than the current international optimal constraints. This may be because the experimental scheme is designed specifically for the Lorentz violating effect of the purely gravitational part, while the current optimal constraints for $d = 8$ are based on experimental data derived from the testing of other theoretical models. The involved experiments are sensitive to the testing of other theoretical models but insensitive to the Lorentz violation effect. In the future, we can focus on studying the characteristics of the $d = 8$ Lorentz violation effect and design more targeted experimental test schemes. Furthermore, this scheme can be extended to the testing of Lorentz violation effects in higher mass dimensions, in order to comprehensively explore the laws of the Lorentz violation effect.

Author Contributions: Conceptualization, C.-G.S. and Y.-J.T.; methodology, C.-G.S., Y.-J.T. and T.J.; software, J.-R.L. and Y.-J.T.; validation, T.J. and J.-R.L.; formal analysis, T.J. and J.-R.L.; investigation, T.J.; resources, C.-G.S. and Y.-J.T.; data curation, T.J. and J.-R.L.; writing—original draft preparation, T.J.; writing—review and editing, Y.-J.T., P.-P.W. and C.-G.Q.; visualization, T.J. and J.-R.L.; supervision, Y.-J.T.; project administration, C.-G.S.; funding acquisition, C.-G.S., Y.-J.T. and C.-G.Q. All authors have read and agreed to the published version of the manuscript.

Funding: This research was funded by the National Natural Science Foundation of China (Grants No. 12175076, No. 11925503, No. 12305062 and No. 12150012) and the Guangdong Major Project of Basic and Applied Basic Research (Grant No. 2019B030302001).

Data Availability Statement: The original contributions presented in the study are included in the article; further inquiries can be directed to the corresponding author.

Acknowledgments: The authors thank Shan-Qing Yang, Wen-Hai Tan, Lin Zhu and Wen-Can Dong for their helpful suggestions and discussions. We are very grateful to the reviewers and editors for their contributions to improving this paper.

Conflicts of Interest: The authors declare no conflicts of interest.

References

1. Nambu, Y. Quantum Electrodynamics in Nonlinear Gauge. *Prog. Theor. Phys. Suppl.* **1968**, *E68*, 190–195. [CrossRef]
2. Amelino-Camelia, G.; Ellis, J.; Mavromatos, N.E.; Nanopoulos, D.V. Distance Measurement and Wave Dispersion in a Liouville-String Approach to Quantum Gravity. *Int. J. Mod. Phys. A* **1997**, *12*, 607–623. [CrossRef]
3. Ellis, J.; Mavromatos, N.E.; Nanopoulos, D.V. Quantum-Gravitational Diffusion and Stochastic Fluctuations in the Velocity of Light. *Gen. Relativ. Gravit.* **2000**, *32*, 127–144. [CrossRef]
4. Amelino-Camelia, G.; Majid, S. Waves on noncommutative space–time and gamma-ray bursts. *Int. J. Mod. Phys. A* **2000**, *15*, 4301–4323. [CrossRef]
5. Alfaro, J.; Morales-Técotl, H.A.; Urrutia, L.F. Loop quantum gravity and light propagation. *Phys. Rev. D* **2002**, *65*, 103509. [CrossRef]
6. Gambini, R.; Pullin, J. Nonstandard optics from quantum space-time. *Phys. Rev. D* **1999**, *59*, 124021. [CrossRef]
7. Alfaro, J. Quantum Gravity and Lorentz Invariance Violation in the Standard Model. *Phys. Rev. Lett.* **2005**, *94*, 221302. [CrossRef] [PubMed]
8. Ellis, J.; Mavromatos, N.E.; Nanopoulos, D.V. Microscopic recoil model for light-cone fluctuations in quantum gravity. *Phys. Rev. D* **1999**, *61*, 027503. [CrossRef]
9. Debono, I.; Smoot, G.F. General Relativity and Cosmology: Unsolved Questions and Future Directions. *Universe* **2016**, *2*, 23. [CrossRef]
10. Kostelecký, V.A.; Samuel, S. Spontaneous breaking of Lorentz symmetry in string theory. *Phys. Rev. D* **1989**, *39*, 683–685. [CrossRef]
11. Amelino-Camelia, G. Quantum-Spacetime Phenomenology. *Living Rev. Relativ.* **2013**, *16*, 5. [CrossRef] [PubMed]
12. Carroll, S.M.; Harvey, J.A.; Kostelecký, V.A.; Lane, C.D.; Okamoto, T. Noncommutative Field Theory and Lorentz Violation. *Phys. Rev. Lett.* **2001**, *87*, 141601. [CrossRef] [PubMed]
13. Bjorken, J.D. Cosmology and the standard model. *Phys. Rev. D* **2003**, *67*, 043508. [CrossRef]
14. Cline, J.M.; Valcárcel, L. Asymmetrically warped compactifications and gravitational Lorentz violation. *J. High Energy Phys.* **2004**, *2004*, 032. [CrossRef]
15. Tasson, J.D. What do we know about Lorentz invariance? *Rep. Prog. Phys.* **2014**, *77*, 062901. [CrossRef]
16. KosteleckÝ, V.A.; Russell, N. Data tables for lorentz and cpt violation. In Proceedings of the Fourth Meeting on CPT and Lorentz Symmetry, Bloomington, IN, USA, 8–11 August 2007; pp. 308–321. [CrossRef]
17. Sanner, C.; Huntemann, N.; Lange, R.; Tamm, C.; Peik, E.; Safronova, M.S.; Porsev, S.G. Optical clock comparison for Lorentz symmetry testing. *Nature* **2019**, *567*, 204–208. [CrossRef]
18. Illuminati, F.; Lambiase, G.; Petruzziello, L. Spontaneous Lorentz Violation from Infrared Gravity. *Symmetry* **2021**, *13*, 1854. [CrossRef]
19. Kostelecký, V.A.; Mewes, M. Testing local Lorentz invariance with gravitational waves. *Phys. Lett. B* **2016**, *757*, 510–514. [CrossRef]
20. Qin, C.G.; Ke, J.; Li, Q.; Chen, Y.F.; Luo, J.; Tan, Y.J.; Shao, C.G. Testing Lorentz symmetry with space-based gravitational-wave detectors. *Class. Quant. Grav* **2023**, *40*, 205005. [CrossRef]
21. Qin, C.G.; Tan, Y.J.; Shao, C.G. Test of Einstein Equivalence Principle by frequency comparisons of optical clocks. *Phys. Lett. B* **2021**, *820*, 136471. [CrossRef]
22. Flowers, N.A.; Goodge, C.; Tasson, J.D. Superconducting-Gravimeter Tests of Local Lorentz Invariance. *Phys. Rev. Lett.* **2017**, *119*, 201101. [CrossRef] [PubMed]
23. Hohensee, M.A.; Müller, H.; Wiringa, R.B. Equivalence Principle and Bound Kinetic Energy. *Phys. Rev. Lett.* **2013**, *111*, 151102. [CrossRef] [PubMed]
24. Aker, M.; Batzler, D.; Beglarian, A.; Behrens, J.; Berlev, A.; Besserer, U.; Bieringer, B.; Block, F.; Bobien, S.; Bornschein, B.; et al. Search for Lorentz-invariance violation with the first KATRIN data. *Phys. Rev. D* **2023**, *107*, 082005. [CrossRef]
25. Kostelecký, V.A.; Mewes, M. Testing local Lorentz invariance with short-range gravity. *Phys. Lett. B* **2017**, *766*, 137–143. [CrossRef]
26. Weinberg, S.; Dicke, R.H. Gravitation and Cosmology: Principles and Applications of the General Theory of Relativity. *Am. J. Phys.* **1973**, *41*, 598–599. [CrossRef]
27. Kostelecký, A. Gravity, Lorentz violation, and the standard model. *Phys. Rev. D* **2003**, *69*, 105009. [CrossRef]
28. Bailey, Q.G.; Kostelecký, V.A.; Xu, R. Short-range gravity and Lorentz violation. *Phys. Rev. D* **2015**, *91*, 022006. [CrossRef]
29. Yang, S.Q.; Zhan, B.F.; Wang, Q.L.; Shao, C.G.; Tu, L.C.; Tan, W.H.; Luo, J. Test of the Gravitational Inverse Square Law at Millimeter Ranges. *Phys. Rev. Lett.* **2012**, *108*, 081101. [CrossRef]
30. Tan, W.H.; Yang, S.Q.; Shao, C.G.; Li, J.; Du, A.B.; Zhan, B.F.; Wang, Q.L.; Luo, P.S.; Tu, L.C.; Luo, J. New Test of the Gravitational Inverse-Square Law at the Submillimeter Range with Dual Modulation and Compensation. *Phys. Rev. Lett.* **2016**, *116*, 131101. [CrossRef]
31. Long, J.C.; Kostelecký, V.A. Search for Lorentz violation in short-range gravity. *Phys. Rev. D* **2015**, *91*, 092003. [CrossRef]
32. Shao, C.G.; Tan, Y.J.; Tan, W.H.; Yang, S.Q.; Luo, J.; Tobar, M.E.; Bailey, Q.G.; Long, J.C.; Weisman, E.; Xu, R.; et al. Combined Search for Lorentz Violation in Short-Range Gravity. *Phys. Rev. Lett.* **2016**, *117*, 071102. [CrossRef] [PubMed]

33. Shao, C.G.; Chen, Y.F.; Tan, Y.J.; Yang, S.Q.; Luo, J.; Tobar, M.E.; Long, J.C.; Weisman, E.; Kostelecký, V.A. Combined Search for a Lorentz-Violating Force in Short-Range Gravity Varying as the Inverse Sixth Power of Distance. *Phys. Rev. Lett.* **2019**, *122*, 011102. [CrossRef] [PubMed]
34. Shao, C.G.; Tan, Y.J.; Tan, W.H.; Yang, S.Q.; Luo, J.; Tobar, M.E. Search for Lorentz invariance violation through tests of the gravitational inverse square law at short ranges. *Phys. Rev. D* **2015**, *91*, 102007. [CrossRef]
35. Jin, T.; Li, J.R.; Tan, Y.J.; Shao, C.G. Recent Experimental Progress on Probing Lorentz Violation in Pure Gravity for $d = 6$. In Proceedings of the Ninth Meeting on CPT and Lorentz Symmetry, Bloomington, IN, USA, 17–26 May 2022; pp. 188–191. [CrossRef]
36. Kostelecký, V.A.; Tasson, J.D. Constraints on Lorentz violation from gravitational Čerenkov radiation. *Phys. Lett. B* **2015**, *749*, 551–559. [CrossRef]
37. Poisson, E.; Will, C.M. *Gravity: Newtonian, Post-Newtonian, Relativistic*; Poisson, E., Will, C.M., Eds.; Cambridge University Press: Cambridge, UK, 2014. [CrossRef]
38. Kostelecký, V.A.; Mewes, M. Electrodynamics with Lorentz-violating operators of arbitrary dimension. *Phys. Rev. D* **2009**, *80*, 015020. [CrossRef]
39. Shao, C.G.; Chen, Y.F.; Tan, Y.J.; Luo, J.; Yang, S.Q.; Tobar, M.E. Enhanced sensitivity to Lorentz invariance violations in short-range gravity experiments. *Phys. Rev. D* **2016**, *94*, 104061. [CrossRef]
40. Chen, Y.F.; Tan, Y.J.; Shao, C.G. Experimental Design for Testing Local Lorentz Invariance Violations in Gravity. *Symmetry* **2017**, *9*, 219. [CrossRef]